Inorg. Chem. **2002**, *41*, 3628–3637

Decomposition of Silver Carbonate; the Crystal Structure of Two High-Temperature Modifications of Ag_2CO_3

P. Norby*

Department of Chemistry, University of Oslo, N-0315 Oslo, Norway

R. Dinnebier†

Max-Planck-Institute for Solid State Research, D-70569 Stuttgart, Germany

A. N. Fitch

European Synchrotron Radiation Facility, F-38043 Grenoble, France

Received October 30, 2001

High-resolution powder diffraction was used to study the thermal transformation of silver carbonate. A sample of Ag_2CO_3 was heated in a capillary under 4.5 atm CO_2 pressure. The decomposition temperature of silver carbonate to silver oxide is thereby increased, allowing high-resolution synchrotron X-ray powder diffraction patterns of the two high-temperature phases of Ag_2CO_3 to be collected. The structure of the low-temperature (lt) phase was confirmed, and the structures of the two high-temperature phases were determined by direct methods and refined using the Rietveld method: lt-Ag_2CO_3 (295 K) $P2_1/m$, $z = 2$, $a = 4.8521(2)$ Å, $b = 9.5489(4)$ Å, $c = 3.2536(1)$ Å, $\beta = 91.9713(3)°$; β-Ag_2CO_3 (453 K) $P31c$, $z = 6$, $a = 9.1716(4)$ Å, $c = 6.5176(3)$ Å; α-Ag_2CO_3 (476 K) $P\bar{6}2m$, $z = 3$, $a = 9.0924(4)$ Å, $c = 3.3249(1)$ Å. In addition, thermal expansion properties, anisotropic microstrain distributions, and thermal transformations of the three silver carbonate phases and silver oxide are described.

Introduction

The decomposition of silver carbonate, Ag_2CO_3, to metallic silver proceeds via silver oxide, Ag_2O. A reversible thermal transition at ~475 K was observed by Wydeven[1] using DTA. Ashford and Snelson[2] observed changes in the powder diffraction patterns of Ag_2CO_3 during heating and cooling. It was later recognized[3] that before the decomposition of silver carbonate to silver oxide, two high-temperature modifications of Ag_2CO_3 exist. The high-temperature form has been named α-Ag_2CO_3 whereas the intermediate temperature phase is called β-Ag_2CO_3.

A number of studies of the decomposition of silver carbonate have been published. Sawada et al. have studied the phase transitions and decomposition using thermal analysis, high-temperature diffraction, and gas analysis.[4−8] A combined in situ XAFS and DSC study of the decomposition of silver carbonate to silver oxide has been published,[9] and surface studies of the decomposition have been performed[10,11] using XPS, ISS, and ELS.

The room-temperature structure of silver carbonate was determined from single-crystal diffraction data.[12] The structure was found to be monoclinic, space group $P2_1/m$, $a = 4.852(4)$ Å, $b = 9.553(8)$ Å, $c = 9.553(8)$ Å, and $\beta = 91.96°$.

* To whom correspondence should be addressed. E-mail: poul.norby@kjemi.uio.no.

† E-mail: r.dinnebier@fkf.mpg.de.

(1) Wydeven, T. *Aust. J. Chem.* **1967**, *20*, 2751.
(2) Ashford, N. A.; Snelson, A. *J. Chem. Phys.* **1969**, *51*, 532−538.
(3) van Hattum, W. Joint Commision on Powder Diffraction Standards, 31-1236, 31-1237.
(4) Sawada, Y.; Mizutani, N.; Kato, M. *Thermochim. Acta* **1989**, *143*, 319−324.
(5) Sawada, Y.; Mizutani, N.; Kato, M. *Thermochim. Acta* **1989**, *146*, 177−185.
(6) Sawada, Y.; Watanabe, N.; Hemni, H.; Mizutani, N.; Kato, M. *Thermochim. Acta* **1989**, *138*, 257−265.
(7) Sawada, Y.; Manabe, K. *J. Therm. Anal.* **1991**, *37*, 1657−1663.
(8) Sawada, Y.; Kanou, N.; Mizutani, N. *Thermochim. Acta* **1991**, *183*, 279−287.
(9) Troger, L.; Hillebrandt, N.; Epple, M. *J. Phys. IV* **1997**, *7*, 323−324.
(10) Salaita, G. N.; Hazos, Z. F.; Hoflund, G. B. *J. Electron Spectrosc. Relat. Phenom.* **2000**, *107*, 73−81.
(11) Epling, W. S.; Hoflund, G. B.; Salaita, G. N. *J. Phys. Chem. B* **1998**, *102*, 2263−2268.
(12) Masse, R.; Guitel, J. C.; Durif, A. *Acta Crystallogr.* **1979**, *B35*, 1428−1429.

10.1021/ic0111177 CCC: $22.00
Published on Web 06/11/2002

An earlier approximate structural model was suggested[13] in $P2_1$.

The powder diffraction patterns of the two high-temperature modifications of silver carbonate observed by Van Hattum[3] were indexed on the basis of hexagonal unit cells: β-Ag_2CO_3, $a = 9.18$ Å and $c = 6.485$ Å (423 K, 4.5 bar CO_2) and α-Ag_2CO_3, $a = 9.094$ Å and $c = 3.329$ Å (483 K, 4.5 bar CO_2). The proposed space groups were $P31c$ and $P\bar{6}$ for the β- and α-modification, respectively. The existence of the two phases was confirmed by Sawada et al.[4−8] However, the crystal structures of the high-temperature modifications have not been determined.

The present study was undertaken in order to determine the crystal structure of the two high-temperature modifications of silver carbonate and to study the thermal expansion properties of the three phases of Ag_2CO_3. In addition, the structural changes leading up to the decomposition to silver oxide were followed, and the thermally induced structural changes of silver oxide before the final decomposition to metallic silver were investigated.

Experimental Section

The sample of silver carbonate, Ag_2CO_3 (Merck p.a.), was used without further purification. Preliminary temperature resolved in-situ powder diffraction experiments were performed at the Chemistry beamline X7B at the National Synchrotron Light Source (NSLS) at Brookhaven National Laboratory (BNL). The sample of silver carbonate was contained in a 0.5 mm quartz glass capillary and was heated using a hot air blower from 298 to 873 K. Temperature resolved powder diffraction data were collected using a translating imaging plate (TIP) system, where an imaging plate is translated horizontally behind a steel screen with a vertical 3 mm slit.[14,15] The wavelength used was 0.9374 Å.

Powder diffraction data were collected at the high-resolution powder diffractometer at BM16 at the European Synchrotron Radiation Facility (ESRF). At BM16, the X-rays from the bending magnet source are collimated vertically by a rhodium-coated silicon mirror before they are incident on the double crystal monochromator.[16] A Si 111 reflection was used to select an X-ray energy of 24 keV. The size of the beam was adjusted to 2×0.6 mm^2 using slits. The wavelength was determined to 0.49121(2) Å from a silicon standard. The sample was contained in a 0.7 mm lithiumborate glass (glass no. 50) capillary and was filled under a flow of carbon dioxide. The capillary was mounted in a Swagelok T-piece fitting using a Vespel/graphite ferrule.[14] The fitting was mounted on a standard goniometer head, and a 4 atm carbon dioxide pressure was applied to the sample via a 1/16 in. Teflon tube. The sample was oscillated ∼90° in order to improve randomization of the crystallites. The diffracted beam was analyzed with a nine crystal analyzer stage (nine Ge(111) crystals separated by 2° intervals) and detected with nine Na(Tl)I scintillation counters simultaneously. The incoming beam was monitored by an ion chamber for normalization for the decay of the primary beam. In this parallel beam configuration, the resolution is determined by the analyzer crystal instead of by slits.[17] Details of the experimental setup are described in the beamline handbook and on the Web (http://www.esrf.fr/).

Data were taken at several temperatures in continuous mode and later normalized and converted to step scan data in steps of 0.005° in 2θ. For the high-temperature scans, a hot air blower[18] manufactured by CNRS (Laboratoire de Cristallographie, BP166, 38042 Grenoble Cedex 09) was used with a temperature stability of less than 1 K for the investigated temperature range.

Low angle diffraction peaks had a fwhm of 0.01° in 2θ for all phases, significantly broader than the resolution of the spectrometer, which is estimated to be as low as 0.002° in 2θ for the given energy.

Powder diffraction data for the structure determination and Rietveld refinement were collected from −7.8° to 53° in 2θ at 373, 398, 423, 438, 453, and 476 K. Data for refinement in order to determine the thermal expansion properties were collected from 5° to 25° in 2θ. Data were collected at various temperatures: 298−338 K, increment 10 K, 338−378K increment 5 K, 378−418 K increment 10 K, 418−443 K increment 5 K, 443−478 K increment 1, 2, or 3 K, 478−523 K increment 5 K, 523−723 K increment 10 K.

Rietveld refinement and LeBail extraction were performed using the program system GSAS.[19] In the analyses, a pseudo-Voigt profile function was used, with anisotropic line broadening modeling as described[20] by Stephens. Structure determinations were performed using the EXPO program.[21]

Thermal analysis was performed using a PL Thermal Sciences STA1500 instrument.

Results

Thermal Analysis. The decomposition of silver carbonate, to silver oxide, was investigated using differential thermal analysis (DTA). Figure 1a shows the DTA curves when heating silver carbonate in a nitrogen atmosphere (A) and in a flow of carbon dioxide (B). The decomposition of silver carbonate to silver oxide gives rise to a broad endotherm in the DTA signal at 510 K. A low temperature shoulder on the DTA signal at ∼470 K is visible when the sample is heated in nitrogen. This is associated with the thermal transformations in silver carbonate prior to decomposition. When the sample is heated in a flow of carbon dioxide, the decomposition is shifted to higher temperatures (from ∼510 to 550 K) because of the increased partial pressure of carbon dioxide. The endothermic event at 470 K, associated with the phase transitions, is now separated from the signal from the decomposition, and the structure in the signal indicates that it is composed of two overlapping signals. This is in agreement with the results reported in ref 4. Figure 1b shows the DTA signal when heating the sample to 498 K in CO_2 with subsequent cooling. When cooling, an exothermic signal is observed at ∼450 K, signifying that at least one of the transitions is reversible. The shape of the exothermic signal could be explained by only one transition. The thermal

(13) Donohue, J.; Helmholtz, L. *J. Am. Chem. Soc.* **1944**, *66*, 295−298.
(14) Norby, P. *J. Appl. Crystallogr.* **1997**, *30*, 21−30.
(15) Norby, P. *J. Am. Chem. Soc.* **1997**, *119*, 5215−5221.
(16) Fitch, A. N. *Mater. Sci. Forum* **1996**, *128−131*, 219−222.
(17) Cox, D. E. Powder Diffraction. In *Handbook on Synchrotron Radiation*; Brown, G., Moncton, De. E., Eds.; Elsevier Science Publishers B. V.: Amsterdam, 1991; Vol. 3, Chapter 5.
(18) Argoud, R.; Capponi, J. J. *J. Appl. Crystallogr.* **1984**, *17*, 420−425.
(19) Larson, A. C.; Von Dreele, R. B. *GSAS−General Structure Analysis System*; Los Alamos National Laboratory Report LAUR 86-748; Los Alamos National Laboratory: Los Alamos, NM, 1994 (available by anonymous FTP from mist.lansce.lanl.gov).
(20) Stephens, P. W. *J. Appl. Crystallogr.* **1999**, *32*, 281−289.
(21) Altomare, A.; Burla, M. C.; Camalli, M.; Carrozzini, B.; Cascarano, G. L.; Giacovazzo, C.; Guagliardi, A.; Moliterni, A. G. G.; Polidori, G.; Rizzi, R. *J. Appl. Crystallogr.* **1999**, *32*, 339−340.

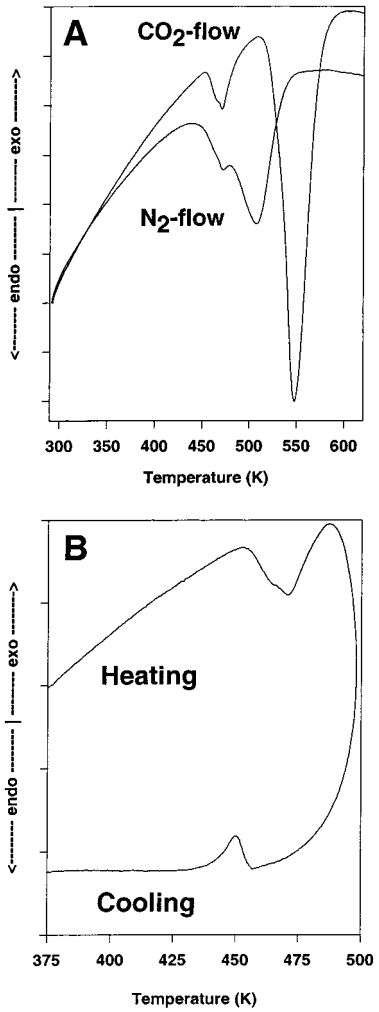

Figure 1. DTA curves for Ag_2CO_3 heated with 5 K/min. (a) Heated to 623 K in nitrogen and in a flow of CO_2. (b) Heated to 498 K and subsequently cooled in a flow of carbon dioxide.

decomposition of silver carbonate was studied earlier[8] using DTA in carbon dioxide pressures from 1 to 40 atm, and similar shifts in the decomposition temperatures were observed. At a carbon dioxide pressure of 40 atm, it was found that the decomposition temperature was shifted by more than 200 K.

In Situ Powder Diffraction. The result from a temperature resolved powder diffraction experiment performed at X7B at NSLS is shown in Figure 2. The sample was heated from 298 to 873 K in a closed quartz glass capillary, and the decomposition from silver carbonate through silver oxide to silver metal is clearly visible. Before the decomposition to silver oxide, two intermediate phases are visible, β- and α-Ag_2CO_3. However, they exist in a very narrow temperature range, and coexistence of the β- and α-phases, and of α-Ag_2CO_3 and silver oxide, is observed. The onset of the transitions and decompositions are in good agreement with the DTA experiments performed in a nitrogen flow.

Another interesting observation from the in situ temperature resolved powder diffraction experiment was the changes in the diffraction pattern of silver oxide with temperature preceding the decomposition to metallic silver. A pronounced narrowing of the diffraction lines with temperature was observed, indicating crystal growth or annealing of defects. In addition, a decrease in the unit cell volume with temperature was observed for Ag_2O.

To determine the crystal structures of the high-temperature phases of silver carbonate, it was necessary to stabilize the pure phases for prolonged periods of time, making it possible to collect high quality powder diffraction data. High-resolution powder diffraction data were collected with the sample under carbon dioxide pressure in order to shift the decomposition to higher temperatures. A powder diffraction pattern for structure analysis was collected at room temperature. The temperature was slowly raised, and at 445 K, a phase transition was observed. The powder diffraction pattern showed that a mixture of β- and α-Ag_2CO_3 was formed. This confirms earlier observations by Sawada et al.,[4,5] who found that β-Ag_2CO_3 does form upon heating, but that a mixture of α- and β-phase is obtained. At 476 K, pure α-Ag_2CO_3 was obtained, and a powder diffraction pattern for structural analysis was collected. The temperature was slowly lowered, and at 453 K, pure β-Ag_2CO_3 was obtained, and a high quality powder diffraction data set was collected. The temperature was slowly lowered, and a mixture of lt- and β-Ag_2CO_3 was obtained. The high-temperature β-Ag_2CO_3 phase was present until room temperature, showing that the phase transition from β-Ag_2CO_3 to the low-temperature phase is very slow. A large structural change combined with the low temperature involved would explain a kinetically hindered phase transition.

Structure Determination. Data reduction was performed using the program GUFI.[22] The pattern of all three phases of Ag_2CO_3 could be indexed using the program ITO[23] with cell parameters given in Table 1.

The peak profiles and precise lattice parameters were determined by LeBail-type fits using the program GSAS.[19] The background was modeled manually using GUFI.[22] The peak profile was described by a pseudo-Voigt function in combination with a special function that accounts for the asymmetry due to axial divergence.[24]

Structure solution for the two high-temperature phases of Ag_2CO_3 was obtained by direct methods using the program EXPO.[21]

Rietveld refinements were carried out using the program GSAS.[19]

lt-Ag_2CO_3. The crystal structure of the low-temperature modification was published[12] by Masse et al. and was refined in a monoclinic unit cell, space group $P2_1/m$.

Indexing of the high-resolution powder diffraction pattern confirmed the monoclinic unit cell. The atomic coordinates from ref 12 were used as starting parameters for the Rietveld refinement, and the refinement confirmed the structure and the space group. Refined atomic coordinates and bond distances are given in Tables 2 and 3. Observed, calculated,

(22) Dinnebier, *R. E. GUFI, a program for measurement and evaluation of powder patterns*; Heidelberger Geowiss. Abh. 68, ISBN 3-89257-067-1, 1993.
(23) Visser, J. W. *J. Appl. Crystallogr.* **1969**, *2*, 69.
(24) Finger, L. W.; Cox, D. E.; Jephcoat, A. P. *J. Appl. Crystallogr.* **1994**, *27*, 892−900.

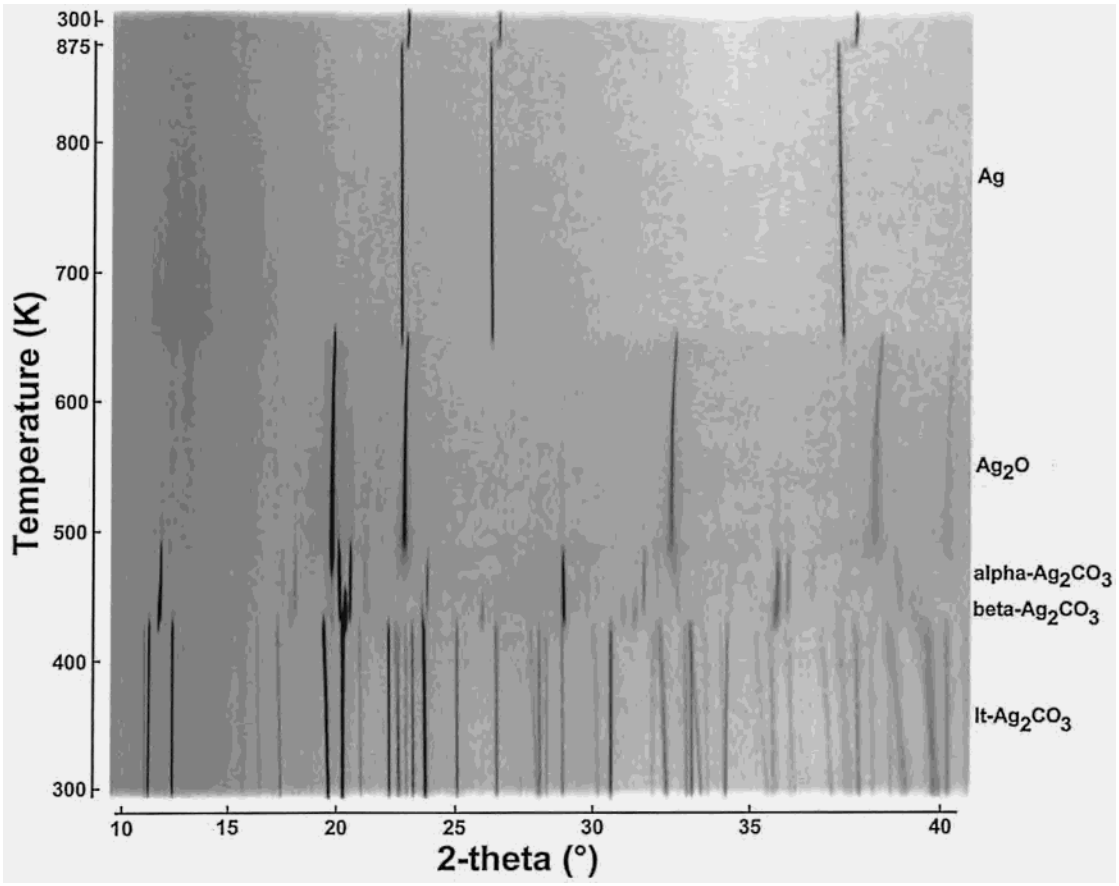

Figure 2. Temperature resolved powder diffraction patterns collected at X7B using a translating imaging plate camera. The sample was contained in a capillary and heated from 298 to 873 K.

Table 1. Crystallographic Data for the Three Phases of Ag_2CO_3 and Ag_2O

	Ag_2CO_3	β-Ag_2CO_3	α-Ag_2CO_3	Ag_2O
temp [K]	295	453	476	623
fw [g/mol]	275.75	275.75	275.75	231.74
space group	$P2_1/m$	$P31c$	$P\bar{6}2m$	$Pn\bar{3}m$
a [Å]	4.8521(2)	9.1716(4)	9.0924(4)	4.7306(2)
b [Å]	9.5489(4)	9.1716(4)	9.0924(4)	4.7306(2)
c [Å]	3.2536(1)	6.5176(3)	3.3249(1)	4.7306(2)
α [deg]	90	90	90	90
β [deg]	91.9713(3)	90	90	90
γ [deg]	90	120	120	90
V [Å^3]	150.66	474.80	238.05	105.87
Z	2	6	3	2
calcd density [g cm^{-3}]	6.079	5.786	5.770	7.270
μ [cm^{-1}] (60% packing)	≈25	≈24	≈24	≈35
capillary diameter [mm]	0.7	0.7	0.7	0.7
2Θ range [deg]	1.0−49.0	2.0−40.1	2.0−35.0	5.12−23.51
step size [deg 2Θ]	0.003	0.003	0.003	0.003
wavelength [Å]	0.49121(2)	0.49121(2)	0.49121(2)	0.49121(2)
fwhm$_{min}$ [deg 2Θ]	0.0106	0.0109	0.0113	0.0101
R-p [%][a]	7.9	5.5	5.5	15.3
R-wp [%]	10.0	8.0	7.6	19.4
R-F^2 [%]	7.5	9.6	6.9	3.1

[a] R-P, R-wp, and R-F^2 refer to the Rietveld criteria of fit for profile, weighted profile, and Bragg R-value, respectively, defined in ref 27. Unit cell parameter esd's are calculated from esd on wavelength. See also ref 28.

and difference powder patterns from the Rietveld refinement are presented in Figure 3a.

Table 2. Positional Parameters and U_i/U_e [Å^2 × 10^3] Values

name	x/a	y/b	z/c	$U_i/U_e \times 10^2$
Low-Temperature Phase of Ag_2CO_3 in $P21/m$ Symmetry at 295 K				
Ag	.21142(8)	.07801(4)	.2188(2)	2.83(3)
C	−0.0219(8)	1/4	.8900(13)	.3(1)
O(1)	.3889(5)	.6362(3)	.3301(9)	−0.11(8)
O(2)	.2666(13)	3/4	.2643(26)	.1(2)
High-Temperature Phase β-Ag_2CO_3 in $P31c$ Symmetry at 453 K				
Ag(1)	.0157(6)	.6821(4)	1/2	6.4(3)
Ag(2)	.6457(3)	.6748(4)	.2529(12)	7.4(2)
C(1)	0	0	.8930(13)	−1.3(2)
O(1)	.0899(9)	.1564(3)	.8930(13)	−1.3(2)
C(2)	2/3	1/3	.2162(19)	3.8(4)
O(2)	.7474(8)	.4903(3)	.2162(19)	3.8(4)
C(3)	2/3	1/3	.7279(20)	2.6(3)
O(3)	.8204(3)	.4378(8)	.7279(20)	2.6(3)
High-Temperature Phase α-Ag_2CO_3 in $P\bar{6}2m$ Symmetry at 476 K				
Ag(1)	.3510(3)	0	0	7.1(2)
Ag(2)	.6799(3)	0	1/2	7.8(2)
C(1)	0	0	0	4.7(14)
O(1)	.0797(11)	.1614(3)	0	−0.2(3)
C(2)	1/3	2/3	1/2	2.4(8)
O(2)	.4859(4)	.7035(11)	1/2	8.7(3)
Ag_2O in $Pn\bar{3}m$ Symmetry at 623 K				
Ag	0	0	0	11.4(1)
O	1/4	1/4	1/4	7.3(6)

***β*-Ag_2CO_3.** A powder diffraction pattern of pure β-Ag_2CO_3 phase was obtained at 453 K. The only way to obtain the pure β-phase was by heating the sample to above 473 K, thus obtaining the pure α-phase, and then cooling it slowly until it transformed into the β-phase. At 453 K, no trace of either α-phase or the low-temperature phase was observed.

Table 3. Selected Bond Lengths [Å] of the Different Phases of Ag_2CO_3 and Ag_2O[a]

	lt-Ag_2CO_3	β-Ag_2CO_3	α-Ag_2CO_3	Ag_2O
C−O(1)	1.273(6)	1.247(2)	1.271(2)	
C−O(2)	1.253(3)	1.247(2)	1.253(2)	
C−O(3)		1.2467(20)		
Ag−Ag (min)	2.8731(8)	3.186(5)	3.32494(2)	3.34505(4)
O−O (min)	2.186(4)	2.159(3)	2.201(4)	
Ag−C (min)	3.147(1)	3.071(3)	3.389(1)	
Ag−O(1)	2.245(3)	3.190(8) (3×)	3.444(8) (2×)	2.04841(2)
	2.986(4)	3.364(9) (3×)	2.179(9) (2×)	
	3.280(1)	2.090(6) (3×)		
Ag−O(2)	3.410(3)	2.871(9) (3×)	2.438(3) (4×)	
	3.353(3)	2.410(8) (3×)		
	2.738(3)			
	2.455(2)			
	2.244(3)			
Ag−O(3)		2.579(10) (3×)		
		2.534(9) (3×)		

[a] The given esd's are Rietveld statistical estimates and should be multiplied by a factor of 6 as discussed in ref 28.

This is in agreement with earlier reports.[3−5] The diffraction pattern of β-Ag_2CO_3 could be indexed on the basis of a trigonal unit cell. Systematic extinctions were in agreement with space groups $P31c$ and $P\bar{3}1c$ for the β-phase of Ag_2CO_3. The structure was solved using direct methods with the program EXPO,[21] and the most promising solution was found using $P31c$. The silver, carbon, and most of the oxygen atoms were found using direct methods. The coordinates for the partial structure were used as starting parameters in the subsequent Rietveld refinement using GSAS. The last atoms were located from difference Fourier maps. Rietveld refinements were initially performed using geometric constraints on the carbonate ion. The constraints were gradually released, and the final refinement was performed without constraints. However, the carbonate groups were restrained to be flat in order to avoid instabilities in the refinement. The final refined coordinates, bond distances, and angles are given in Tables 2 and 3. Observed, calculated, and difference powder diffraction patterns are shown in Figure 3b.

Closer inspection of the powder pattern of the β-phase of Ag_2CO_3 revealed several very weak reflections violating $P31c$ symmetry, indicating $P3$ as the true symmetry of this phase. Rietveld refinements in $P3$ did not improve the fit but led to instabilities in the refinement due to the strongly increased number of parameters and extremely small atomic shifts away from symmetry related positions in $P31c$ symmetry. We therefore present the crystal structure of β-Ag_2CO_3 in the higher symmetry space group.

α-Ag_2CO_3. The powder diffraction pattern of pure α-Ag_2CO_3 was collected at 476 K. The pattern was indexed on the basis of a hexagonal unit cell. No systematic extinctions were found, leaving eight trigonal and eight hexagonal possible space groups. Although several space groups for the α-phase of Ag_2CO_3 were much less likely than the others, all 16 space groups were tried systematically, clearly indicating $P\bar{6}2m$ as the correct space group. This is in contrast to the space group $P\bar{6}$ proposed by van Hattum.[3]

The structure was solved using EXPO.[21] Two crystallographic independent silver cations and two carbonate anions were located. Subsequent Rietveld refinements indicated oxygen disorder in one of the carbonate anions (O1). The final refined coordinates, bond distances, and angles are given in Tables 2 and 3. Observed, calculated, and difference powder diffraction patterns are shown in Figure 3c.

Table 4. Thermal Expansion Coefficients for the Three Phases of Silver Carbonate

	$10^5\,\alpha_a\,K^{-1}$	$10^5\,\alpha_b\,K^{-1}$	$10^5\,\alpha_c\,K^{-1}$	$10^5\,\alpha_V\,K^{-1}$
lt-Ag_2CO_3 295−460 K	2.4	−0.5	7.4	9.1
β-Ag_2CO_3 295−460 K	300 K: −1.4 350 K: −0.6 450 K: −3.8		12.1	8.7
α-Ag_2CO_3 460−575 K	−0.5		7.3	6.2

Strain Anisotropy. The high resolution of the powder patterns of the three phases of Ag_2CO_3 revealed misfits between the calculated and observed powder profiles due to anisotropic peak broadening. We used the model developed by Stephens[20] as implemented in GSAS for the analysis of the lattice strain. A three-dimensional representation of the lattice strain for the three phases of Ag_2CO_3 is given in Figure 4, showing that the overall amount of strain as well as the strain anisotropy decreases considerably from the low-temperature to the β-phase, whereas it increases again from the β- to the α-phase.

The occurrence of slightly negative temperature factors for some atoms in the refinement indicates the presence of additional disorder, which has not been accounted for by the present structural models. However, the excellent agreement between the measured and the calculated profile after the final refinement for all three phases of Ag_2CO_3 indicates that further refinement might not reveal more structural details.

Thermal Expansion. The thermal expansion properties of the three silver carbonate phases (see Table 4) and of silver oxide formed by the decomposition were determined. Powder diffraction data were collected during heating and cooling. Unit cell parameters were determined by Rietveld refinement using the program GSAS.

Figure 5 shows the thermal expansion of the low-temperature modification of silver carbonate. Powder diffraction data were collected for the pure phase during heating and for the mixture of lt- and β-Ag_2CO_3 during cooling. The b-axis shows a very small negative thermal expansion while the a- and c-axes display a positive thermal expansion. The relative thermal expansion of the c-axis is approximately twice that of the a-axis. The anisotropic thermal expansion is also recognized in Figure 2 as diffraction lines split and cross each other.

Figure 6 shows the thermal expansion of β- and α-Ag_2CO_3. To compare the unit cell parameters, the c-axis of β-Ag_2CO_3 has been divided by 2. The a-axis for both phases shows a very small negative thermal expansion, while the c-axis displays normal positive thermal expansion. A discontinuity in the unit cell parameters is observed for both axes at the phase transformation.

In Figure 7, the normalized unit cell volumes of the three Ag_2CO_3 phases as a function of temperature are shown. The

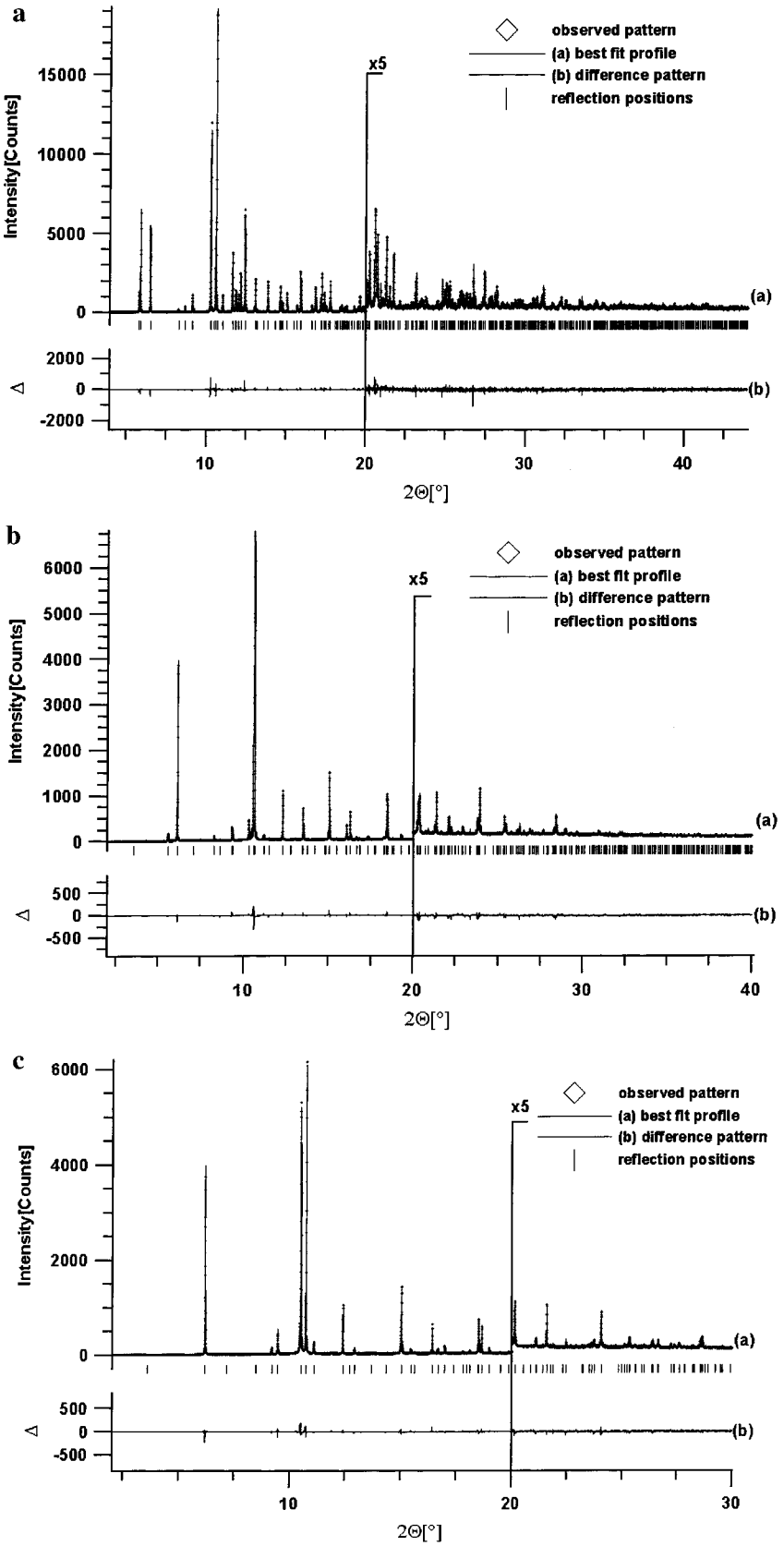

Figure 3. Scattered X-ray intensity for (a) lt-Ag_2CO_3 at 25 °C, (b) β-Ag_2CO_3 at 453 K, and (c) α-Ag_2CO_3 at 476 K as a function of diffraction angle, 2θ. Shown are the observed patterns ($\diamond$), the best Rietveld-fit profiles (—), and the enlarged difference curves between observed and calculated profiles. The high angle parts are multiplied by a factor of 5, starting at 20° in 2θ. The wavelength was $\lambda = 0.491213(2)$ Å.

unit cell volumes are given per silver cation. The thermal expansion coefficients of the three phases are comparable (9.1×10^{-5}, 8.7×10^{-5}, and 6.2×10^{-5} K^{-1} for the lt-, β-, and α-phases, respectively). The thermal expansion coef-

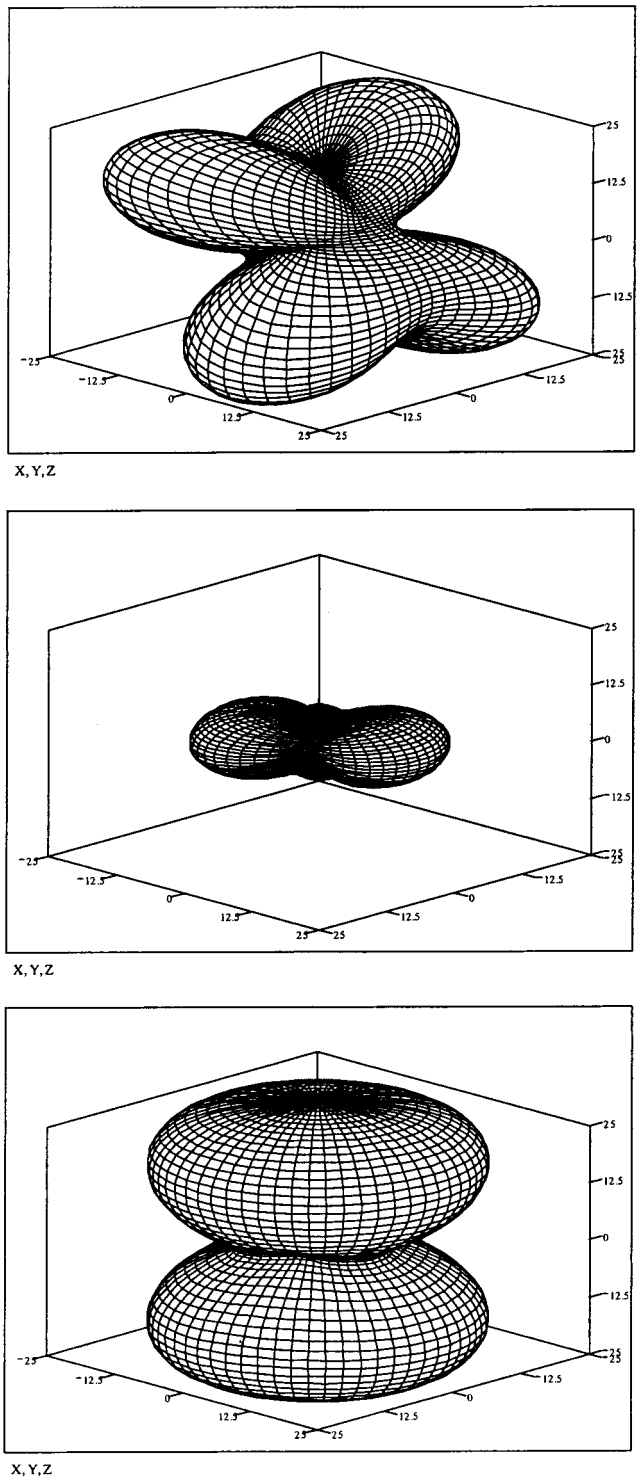

Figure 4. Three-dimensional microstrain distributions of the different phases of Ag_2CO_3 (top, low-temperature phase; middle, β-phase; bottom, α-phase). The *x*-axis is horizontal, *z*-axis, vertical, and the *y*-axis, out of the paper. The scale (in $\delta d/d \times 10^{-6}$ strain) is the same for all phases.

ficients for the lt- and the β-phases are almost identical, while the thermal expansion coefficient of α-Ag_2CO_3 is slightly lower and the thermal expansion is not quite linear.

To investigate the effect of the carbon dioxide pressure on the decomposition temperature of silver carbonate to silver oxide, a sample of Ag_2CO_3 was heated to 775 K in 4.5 atm CO_2. Decomposition to silver oxide was observed at 583 K and was thus significantly shifted to higher temperatures as compared to decomposition in nitrogen (510 K) and 1 atm CO_2 (550 K).

As can be seen from Figure 1, the diffraction peaks of silver oxide shift to lower angles upon heating; that is, the thermal expansion is negative. Silver oxide has a cubic structure, space group $Pn\bar{3}m$. Powder diffraction patterns were collected for silver oxide up to the decomposition to metallic silver at 700 K. Above 625 K, a splitting of the diffraction peaks was observed. Rietveld refinement of the silver oxide structure could be performed using two slightly different cubic unit cells. No difference in composition was revealed by the refinement, but neutron diffraction would be necessary for reliable determination of any nonstoichiometry. The cubic unit cell parameters as a function of temperature between 565 and 700 K are shown in Figure 8. The thermal expansion is negative and nonlinear.

Discussion

Structural similarities between silver and alkali metal salts are not unusual. Especially, sodium and silver salts often have comparable structures, because of similar charge, size, and oxygen coordination requirements. However, the crystal structures of the different phases of silver carbonate are different from those of most alkali carbonates known so far (ref 25 and references therein). A characteristic feature of the crystal structures of α-, β-, γ-Na_2CO_3, α-, β-, γ-K_2CO_3, Rb_2CO_3, and Cs_2CO_3 is that the cations and the complex anions are stacked along the crystallographic *c*-axis. The carbonate anions are stacked alternating with alkali cations forming columns. Between these columns are stacks composed of only alkali cations. The coordination around the alkali metal ions is quite different in the different structures of the alkali carbonates, and only a few direct group−subgroup relations exist. Nevertheless, the general arrangements of the cations and anions are similar, with a clearly visible hexagonal pseudosymmetry. The main reason for the structural differences lies in the increasing size of the cation in the higher alkali homologues. To accommodate for the increasing demand of space, the cation stacks deviate from linearity (angle between cations of 180°) to zigzag chains with a maximal deviation from linearity of 26° for cesium carbonate. In addition, the CO_3^{2-} anions bend either uniformly or alternatingly out of the crystallographic *ab*-plane. It should be mentioned that two polymorphs of sodium carbonate show modulated crystal structures.

The low-temperature structure of silver carbonate is different. It is built from stacks entirely composed of silver cations or carbonate anions. The structure is more related to lithium carbonate, where a similar stacking of cations and anions is found.[26] However, in lithium carbonate, the orientation of the carbonate anions is alternating. Figure 9

(25) Feldmann, C.; Jansen, M. *Z. Kristallogr.* **2000**, *215*, 343−345.
(26) Effenberger, H.; Zemann, J. *Z. Kristallogr.* **1979**, *150*(1−4), 133−138.
(27) Langford, I.; Louër, D. *Rep. Prog. Phys.* **1996**, *59*, 131−234.
(28) Hill, R. J.; Cranswick, L. D. M. *J. Appl. Crystallogr.* **1994**, *27*, 802−844.

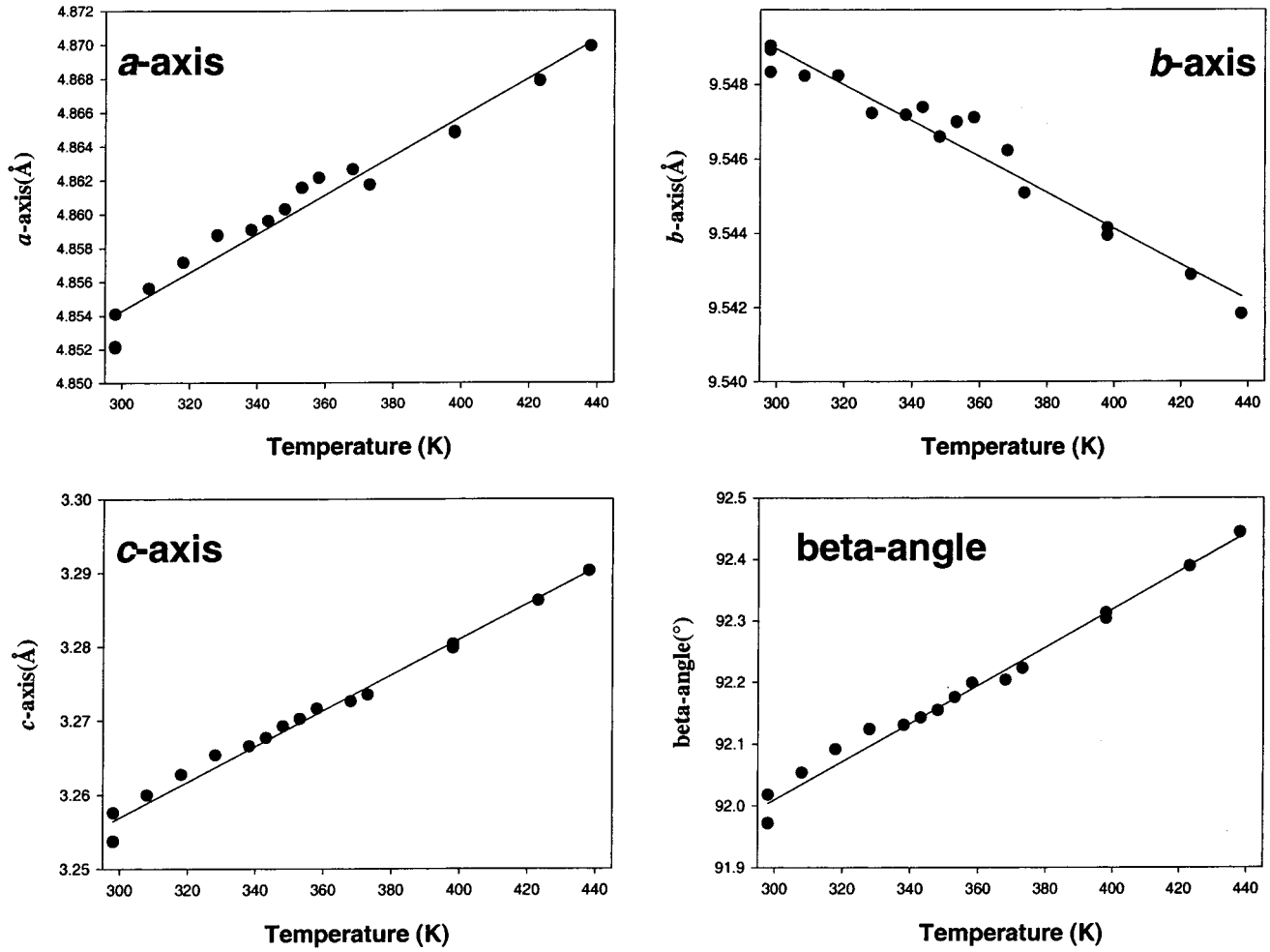

Figure 5. Unit cell parameters as a function of temperature for the low-temperature modification of silver carbonate.

shows projections approximately perpendicular to the planes of the carbonate anions of the crystal structures of Na_2CO_3 and the three polymorphs of Ag_2CO_3.

High-temperature modifications usually have higher symmetry and/or fewer atoms in the asymmetric unit. In the case of silver carbonate, the space group symmetry is indeed higher for the high-temperature phases, going from monoclinic to hexagonal symmetry. However, whereas there is only one silver cation and one carbonate anion in the asymmetric unit in the low-temperature phase, β-silver carbonate has two symmetry inequivalent silver cations and three carbonate anions. In α-silver carbonate, there are two silver cations and two carbonate anions in the asymmetric unit. A further examination of the structures is necessary in order to understand the reason for this increase in the number of symmetrically inequivalent atoms.

In the low-temperature monoclinic structure of silver carbonate, the carbonate anions are not perpendicular to the *c*-axis. The arrangement of the stacks of carbonate anions, when viewed in projection, has almost hexagonal symmetry. Six carbonate anions and six silver cations surround each carbonate anion. However, the arrangement cannot have hexagonal symmetry, because of the mirror plane perpendicular to the *b*-axis. As can be seen from Figure 9, the arrangement of silver cations around a carbonate group could be described as UD−UD−P−UD−UD−P, where UD means $^1/_2$ *c*-axis up and down and P means in the same plane. The silver cation is coordinated to four oxygen atoms with Ag−O distances between 2.24 and 2.73 Å. In addition, it has two long oxygen contacts (2.98 and 3.28 Å).

The transition to the partially disordered hexagonal α-silver carbonate reflects a significant structural change. The basic arrangement of stacks of carbonate anions and silver cations, seen in projection, is preserved (Figure 9). However, the carbonate anions are now surrounded by silver cations in a UD−P−UD−P−UD−P arrangement. There are now two symmetry inequivalent carbonate anions. The carbonate anions are planar and perpendicular to the *c*-axis and are, like the silver cations, situated in $z = 0$ and $^1/_2$. However, there are twice as many carbonate groups in the $z = {}^1/_2$ layer than in the $z = 0$ layer because C1 is situated on a higher symmetry position than C2. The two carbonate groups are very different; C1 is surrounded by six C2 carbonate groups out of plane, while the C2 groups are surrounded by three C2 groups in plane and three C1 groups out of plane, Figure 9. The resulting weak interactions with the C2 carbonate groups in the same plane lead to easy formation of disorder in the C1 carbonate group.

Upon cooling, a phase transition to the β-phase takes place. Only minor structural rearrangements are involved. The

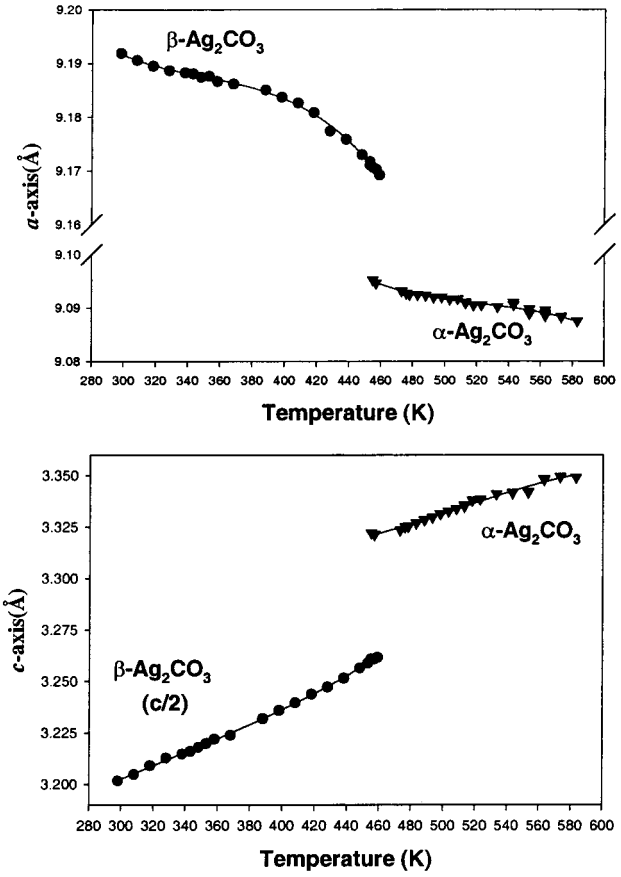

Figure 6. Thermal expansion of β- and α-Ag_2CO_3. To compare the unit cell parameters, the *c*-axis of β-Ag_2CO_3 was divided by 2.

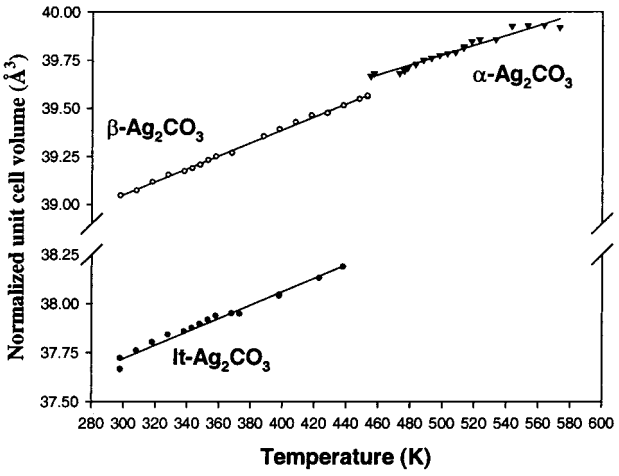

Figure 7. Normalized unit cell volumes of the three Ag_2CO_3 phases as a function of temperature. The unit cell volumes are given in $Å^3$ per silver cation.

overall arrangement of the silver cations and carbonate anions is the same. However, an alternating rotational ordering of the carbonate anions along the *c*-axis causes a doubling of the *c*-axis. In addition, the carbonate anions and silver cations are no longer in exactly the same plane. A direct supergroup relation exists from the α-Ag_2CO_3 in space group $P\bar{6}2m$ via an unobserved intermediate phase in space group $P31m$ and further on to β-Ag_2CO_3 in space group $P31c$ with doubled *c*-axis. Thus, the structural rearrangement between the α- and the β-phase is mainly due to translation of the silver cations and rotation of the carbonate anions.

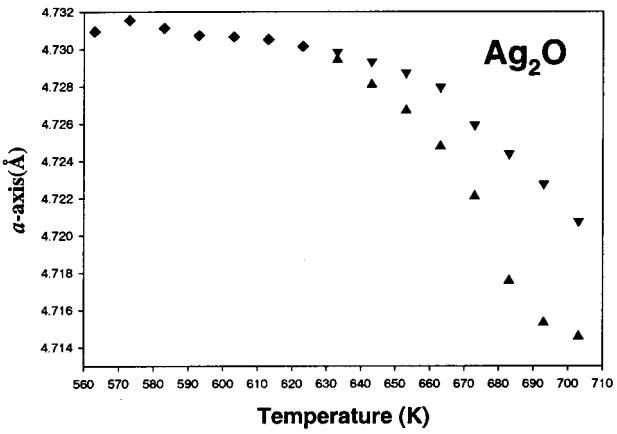

Figure 8. Cubic unit cell parameter for Ag_2O between 565 and 700 K.

The transformation back to the low-temperature phase involves a significant rearrangement of the structure, resulting in a sluggish phase transition. The structural rearrangement of the silver cations from the low-temperature phase to the β-phase may be accomplished by removing the mirror plane and translating the silver cations ca. $+1/4$ and $-1/4$, respectively, along the *c*-axis. However, a significant rearrangement and redistribution of the carbonate groups is involved in the complete transformation. Extensive supercooling of the high-temperature phase is observed with the two phases coexisting down to room temperature. The first-order phase transition from the β-phase of silver carbonate in $P31c$ to the low-temperature phase in $P12_1/m1$ does not follow a direct sub−supergroup relation; for example, the 2_1 screw axis cannot be found in the hexagonal space groups. The unit cell of the α-phase can be transformed to that of the low-temperature phase by

$$\begin{pmatrix} \frac{1}{2} & \frac{1}{2} & 0 \\ -\frac{1}{3} & \frac{1}{3} & 0 \\ 0 & 0 & \frac{1}{2} \end{pmatrix}$$

and a shift of origin of

$$\frac{1}{4}\frac{1}{4}\frac{1}{4}$$

The significant structural changes between the low- and the high-temperature phases would also explain why a mixture of α- and β-phase is obtained upon heating, while pure β-Ag_2CO_3 phase can be obtained only by subsequent cooling of the α-phase. The transition of the low-temperature phase takes place at a temperature high enough to form both the ordered and the disordered high-temperature phase. By subsequent cooling, the transition back to the low-temperature phase is kinetically hindered, and the disorder/order transition is observed. Thus, the findings are in agreement with the suggestion by Sawada et al.[4,5] that the β-phase is

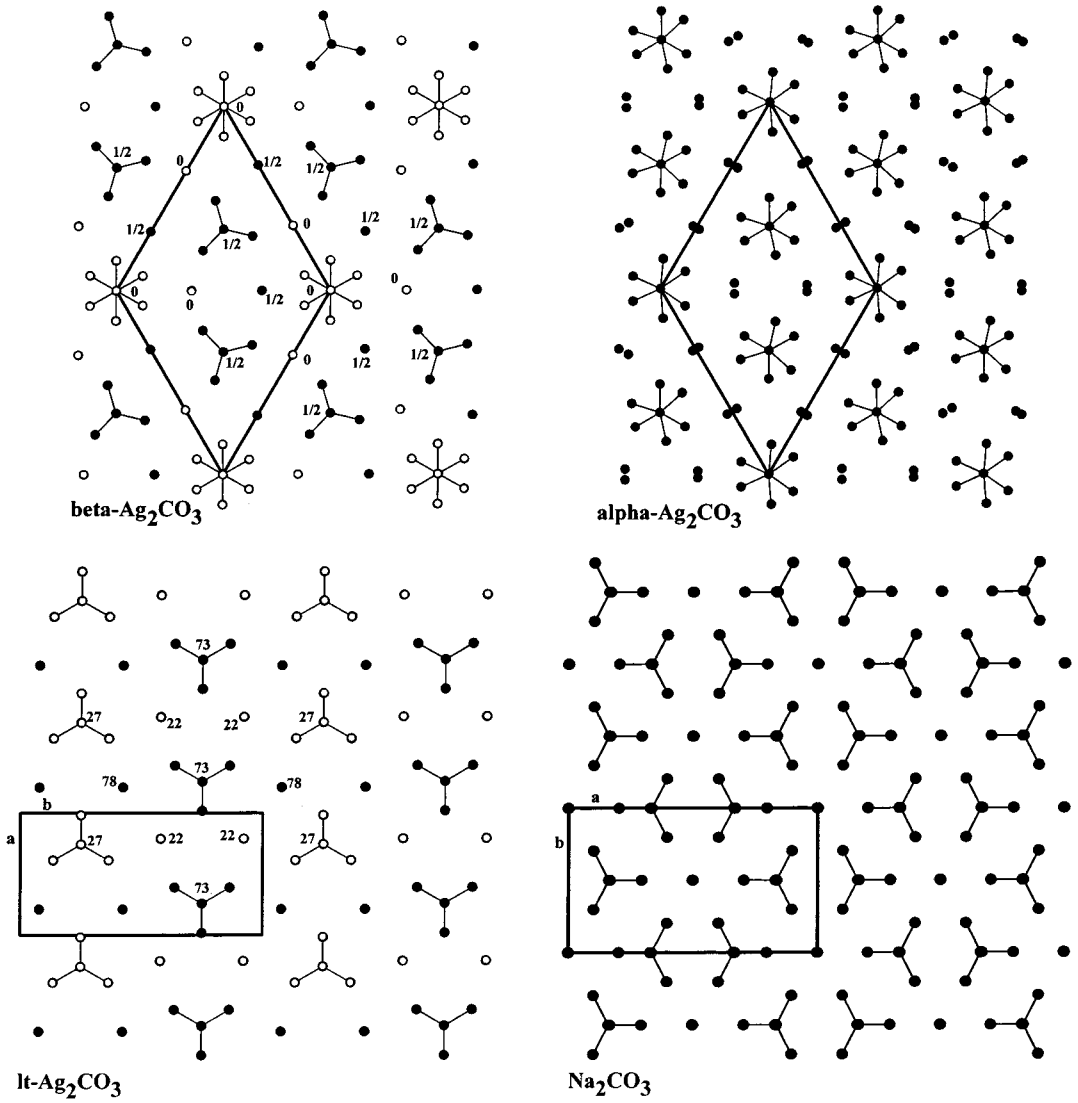

Figure 9. Crystal structures of Na_2CO_3 and the three polymorphs of Ag_2CO_3 shown as projections perpendicular to the carbonate anions. For lt- and β-Ag_2CO_3, the *z*-coordinates for carbon and silver are indicated.

not a process-dependent intermediate phase but a temperature-dependent equilibrium phase.

Acknowledgment. Jonathan C. Hanson is acknowledged for help with collecting the temperature resolved powder diffraction data at X7B. Diffraction measurements at ESRF were carried out under the general user proposal CH-846. Financial support was obtained from the Deutsche Forschungsgemeinschaft (DFG) and the Fonds der Chemischen Industrie (FCI).

Supporting Information Available: Crystallographic information in CIF format. This material is available free of charge via the Internet at http://pubs.acs.org.

IC0111177